Virchows Archiv
https://doi.org/10.1007/s00428-022-03391-8

ORIGINAL ARTICLE

Perivascular infiltration reflects subclinical lymph node metastasis in invasive lobular carcinoma

Akiko Igawa[1,2] · Hiroki Mizukami[1] · Kazuhiro Kudoh[1] · Yuki Takeuchi[1] · Takanori Sasaki[1] · Xuekai Pan[1,2] · Kenichi Hakamada[2]

Received: 12 April 2022 / Revised: 15 July 2022 / Accepted: 26 July 2022

Abstract

Invasive lobular carcinoma (ILC) is characterized by discohesive cells due to irreversible loss of E-cadherin expression and multiple satellites, where individual cell migration is evident without disturbance of the stroma. Neoplastic cells sometimes infiltrate the surrounding vessel in satellites. Here, we aimed to clarify the specific role of perivascular infiltration (PVI) and ameboid migration, characterized by nondisturbance of the background stromal structure, in ILCs. A total of 139 cases with ILC and 122 cases with invasive breast carcinoma of no special type (IBC-NST) were evaluated retrospectively. PVI was significantly more common in ILC than in IBC-NST (50% [70 of 139 cases] vs. 9% [11 of 122 cases], $p < 0.001$). ILC cases with PVI showed a larger pathological tumour size than clinical tumour size ($p < 0.01$), a higher frequency of pathological node status pN2-pN3 when limited to clinically node-negative cases ($p < 0.01$) and lower circularity of tumour morphology on imaging ($p < 0.01$) than ILC cases without PVI. In the pathological evaluation, the intensity and occupancy of tumour cells expressing phospho-myosin light chain 2, which is a hallmark of ameboid migration, were significantly higher in ILC cases with PVI than in those without PVI at the tumour margins ($p < 0.05$). ILC with PVI is associated with irregular, poorly defined tumour margins and lymph node metastasis without adenopathy, which is difficult to assess using imaging. PVI may be caused by ameboid migration, as shown by the positive expression of phospho-myosin light chain 2. The presence of PVI may be a predictor for clinically node-negative pN2-pN3 in ILC patients.

Keywords Invasive lobular carcinoma · Perivascular infiltration · Satellite · Ameboid migration · Myosin II activation

Abbreviations

PVI	Perivascular infiltration
ALND	Axillary lymph node dissection
SLN	Sentinel lymph node
SNB	Sentinel node biopsy
FNAC	Fine-needle aspiration cytology
IBC-NST	Invasive breast carcinoma of no special type
ILC	Invasive lobular carcinoma
ER	Oestrogen receptor
PgR	Progesterone receptor
HER2	Human epidermal growth factor receptor 2
cN(−)	Clinically node negative
cN(+)	Clinically node positive

✉ Hiroki Mizukami
hirokim@hirosaki-u.ac.jp

[1] Department of Pathology and Molecular Medicine, Hirosaki University Graduate School of Medicine, 5 Zaifu-cho, Hirosaki, Aomori 036-8562, Japan

[2] Department of Gastroenterological Surgery, Hirosaki University Graduate School of Medicine, 5 Zaifu-cho, Hirosaki, Aomori 036-8562, Japan

Introduction

Invasive lobular carcinoma (ILC) is pathologically defined as an invasive breast carcinoma composed of discohesive cells, often with loss of expression of cell adhesion molecules, including E-cadherin, individually dispersed patterns or arranged in a single-file linear pattern [1]. The loss of E-cadherin expression is caused primarily by either CDH1 mutations (50 − 60%) or chromosome 16q loss where CDH1 is located [2]. These distinctive pathological findings are assumed to yield unique tumour behaviour and several differences between ILC and invasive breast carcinoma of no special type (IBC-NST). ILC tumours tend to be clinically underestimated and are diagnosed as node-negative on imaging because of a small stromal reaction and no adenopathy [3–5].

Published online: 10 August 2022

In general, there are two modes of individual cell migration in carcinoma: mesenchymal migration, which requires proteolysis towards the surrounding tissue, and ameboid migration in which the high contractile force of actomyosin allows cells to squeeze through tissue gaps without proteolysis [6]. In ILCs, multicellular streaming known as a single-file linear pattern can induce either mesenchymal migration or amoeboid migration [7]. Infiltration without disturbance of the background architecture of ILCs is more reminiscent of amoeboid migration than mesenchymal migration. However, the relationship between histological findings in ILCs and the migration mode has not been clarified.

ILC is characterized by the presence of multiple satellites [1, 4]. Foschini et al. reported that neoplastic cells are frequently observed in perivascular spaces in cases with multiple ILC areas [8]. Other types of malignant tumours, such as glioblastoma and melanoma, are also known to have satellites with vessels. These satellites are referred to as perivascular aggregation or perivascular migration (angiotropism). In these tumours, the perivascular space is assumed to be a track for migration related to tumour progression [9–12], while the significance of perivascular infiltration (PVI) in ILCs is not clear. We hypothesized that ameboid migration could be an important factor in PVI formation, which would explain the unique tumour behaviour of ILCs. In this study, we aimed to clarify the specific role of PVI and amoeboid migration in the unique clinicopathological findings in ILCs.

Materials and methods

Cases

We retrospectively recruited 138 patients, including one patient with bilateral ILC (for a total of 139 cases), who underwent surgery at Hirosaki University Hospital from 2007 to 2017 (Supplemental Table 1). As a control, we analysed 122 patients with IBC-NST, which represented 47% (122/247 cases) of all breast carcinomas, who underwent surgery at Hirosaki University Hospital from 2014 to 2017 (Supplemental Table 1). Following the definition of the WHO classification 5th edition 2019, ILC was histologically diagnosed if an IBC was composed of dispersed or linear discohesive cells while referring to E-cadherin expression (loss of E-cadherin expression in 138 cases and reduction of E-cadherin expression in 1 case). This is because alterations in the integrity of other cadherin complexes can also contribute to discohesiveness in ILCs [1]. We excluded cases with neoadjuvant therapy, synchronous distant metastasis and multiple tumours, including other histologic types, without axillary treatment, after ipsilateral breast-conserving surgery or surgical biopsy. Our study was approved by the Ethics Committee of Hirosaki University Graduate School of Medicine (approval number #2019–119). We disclosed the research content to all participants and obtained consent in an opt-out format.

Clinical examination

The clinical tumour size was defined as the maximum diameter of the enhanced area containing small satellite lesions on magnetic resonance imaging (MRI) or computed tomography (CT) images. In addition to the assessment of pathological tumour size in this study, satellite lesions were included in the clinical tumour size. MRI was performed in 70 of 139 cases with ILC and 98 of 122 cases with IBC-NST. The clinical axillary lymph node status was evaluated based on CT if fine-needle aspiration cytology (FNAC) was not performed. A metastatic lymph node on CT was defined as a short-axis diameter of more than 7 mm and the near absence of intranodal fat density, which were the criteria with high specificity based on a previous report [13]. In addition, a short-axis diameter or maximum cortical thickness was measured as the clinical lymph node size using CT images. In ILC cases, clinical node metastasis was diagnosed by FNAC in only 3 cases that had a short-axis diameter of 7.1–8.0 mm.

Morphology of the tumour in MRI or CT images was quantified by circularity [14] using ImageJ software (ver. 1.52a, NIH, Bethesda, MD, USA). The definition was as follows:

$$\text{Circularity} = 4\pi \cdot \text{Area (mm2)}/\text{Perimeter.2 (mm2)}$$

These values were measured using ImageJ by tracing the tumour borders to include satellite foci. In the case of two solitary masses, the larger mass was evaluated, but 3 or more masses were excluded from the morphological evaluation. The final circularity was the average of each value in two MRI pairs of axial and sagittal images in 68 cases. Circularity was also evaluated in two CT pairs of axial and coronal images in 79 cases. Forty-seven cases (59%) overlapped with cases of MR images.

Histopathologic examination

Histopathological reassessment was performed according to the WHO Classification of Tumours [1]. TNM staging was performed based on the 8th edition of the UICC. We reassessed the histologic type as follows: tumours with > 90% ILC were classified as ILC, and those with > 90% invasive breast carcinoma of no special type were classified as

Table 1 Clinicopathological characteristics of ILC with or without PVI

Characteristics	ILC ($n=139$)		p value
	PVI(−) ($n=69$)	PVI(+) ($n=70$)	
Age (years)	61.0 ± 10.7	59.4 ± 13.2	0.44
Local treatment Partial mastectomy Total mastectomy	50.7% (35/69) 49.3% (34/69)	47.1% (33/70) 52.9% (37/70)	0.74
Clinical tumour size (mm)	25.5 ± 16.9	33.4 ± 15.3	0.005
Pathological tumour size (mm)	23.7 ± 13.9	42.9 ± 25.2	< 0.001
Pathological tumour size - Clinical tumour size (mm)	− 1.9 ± 9.1	9.1 ± 19.8	0.001
Clinical node status Negative Positive	89.9% (62/69) 10.1% (7/69)	94.3% (66/70) 5.7% (4/70)	0.37
Pathological node status Negative Positive	73.9% (51/69) 26.1% (18/69)	62.9% (44/70) 37.1% (26/70)	0.20
Nuclear pleomorphism 1, 2 3	95.7% (66/69) 4.3% (3/69)	98.6% (69/70) 1.4% (1/70)	0.37
Mitotic count 1 2, 3	91.3% (63/69) 8.7% (6/69)	95.7% (67/70) 4.3% (3/70)	0.33
Lymphovascular invasion Negative Positive	88.4% (61/69) 11.6% (8/69)	80.0% (56/70) 20.0% (14/70)	0.25
Pectoral muscle invasion Negative Positive	100% (69/69) 0% (0/69)	95.7% (67/70) 4.3% (3/70)	0.25
Skin invasion Negative Positive	85.5% (59/69) 14.5% (10/69)	88.6% (62/70) 11.4% (8/70)	0.62
Oestrogen receptor Negative Positive	8.7% (6/69) 91.3% (63/69)	4.3% (3/70) 95.7% (67/70)	0.33
HER2 status Negative Positive	98.6% (68/69) 1.4% (1/69)	95.7% (67/70) 4.3% (3/70)	0.62
Ki67 index (%)	19.4 ± 13.4	17.3 ± 11.3	0.34
Histological subtype Classic Nonclassic	76.8% (53/69) 23.2% (16/69)	84.3% (59/70) 15.7% (11/70)	0.29

ILC invasive lobular carcinoma, *PVI* perivascular infiltration, *HER2* human epidermal growth factor receptor 2

IBC-NST. All H&E-stained slides from ILCs and at least two involved sections from IBC-NST cases (IBC-NSTs) were reviewed by AI, KK and HM in a blinded manner. Pathological tumour size was measured microscopically as the largest continuous extent of invasion. The same rule was applied to extensive carcinoma in situ with multiple small invasions (< 10 mm). As an exception to the size rule according to the definition of the latest revised edition of the CAP protocol, if two histologically similar carcinomas were within 5 mm of each other, the size was measured from the outer edges of the two [15].

Table 2 Pathological node status in clinically node-negative ILCs

Node status	PVI (−)	PVI (+)	p value
pN(+)/cN(−)	17.7% (11/62)	33.3% (22/66)	0.068
pN2 + pN3/cN(−)	0% (0/62)	15.2% (10/66)	0.001
pN2 + pN3/cN(−)pN(+)	0% (0/11)	45.5% (10/22)	0.013

PVI perivascular infiltration, *cN* clinical node status, *pN* pathological node status

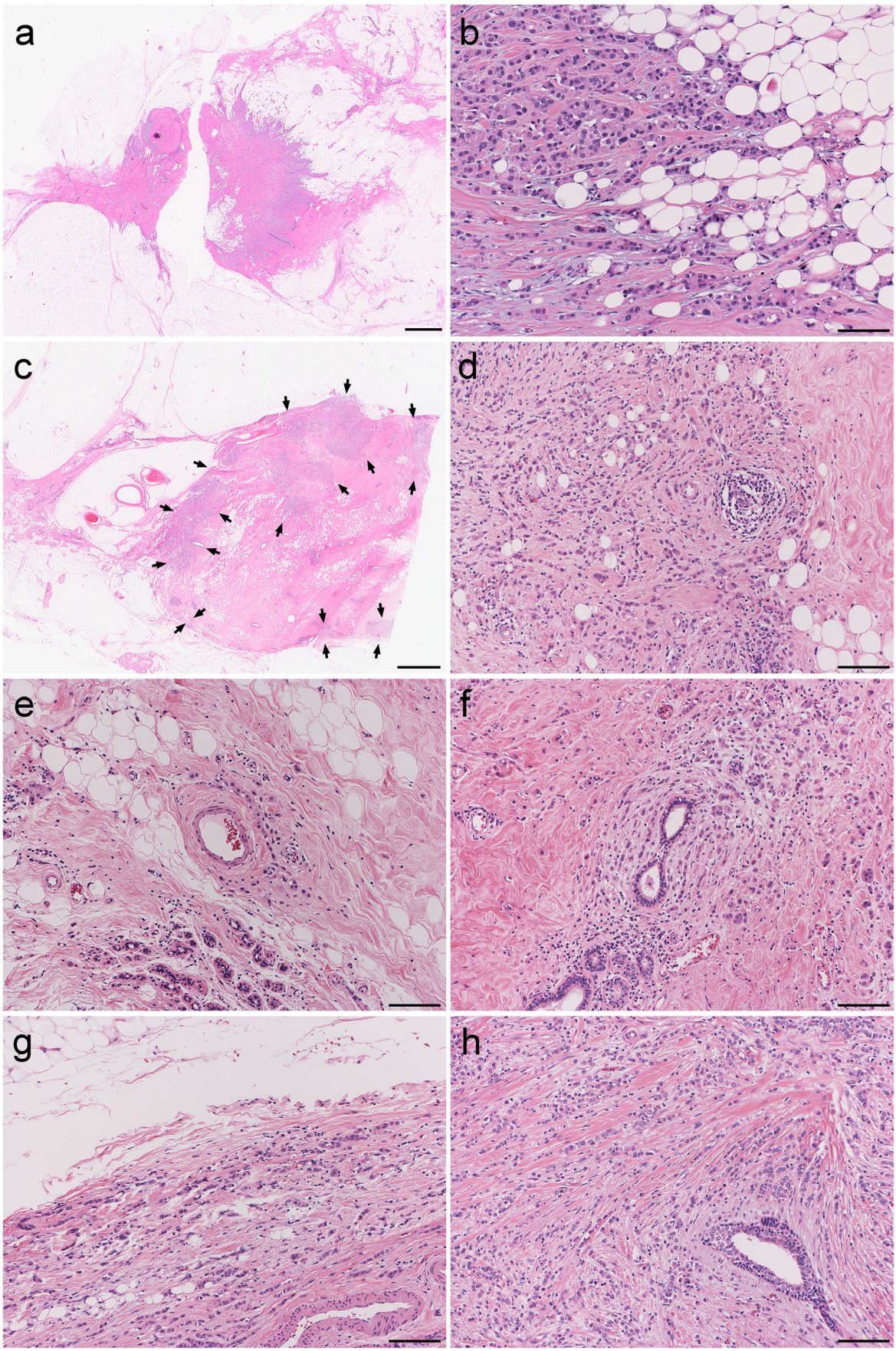
a
b
c
d
e
f
g
h

◂**Fig. 1** Pathological findings in ILCs with PVI. At the border of the tumour, tumour cells invaded the surrounding fatty tissue and remodelled the structure in the PVI-negative case (**a**), which is the same case as shown in Supplemental Fig. 3a. Tumour cells arranged in a single-file linear pattern infiltrated the fatty tissue with a desmoplastic reaction (**b**). In the PVI-positive case, tumour cells predominantly infiltrated the breast collagen structure in the peripheral side of the tumour in the H&E section (arrows) (**c**), which is a corresponding finding observed in the MRI in Supplemental Fig. 3b (red arrow). Tumour cells infiltrated with little disturbance of the background architecture (**d**). Tumour cells arranged in a single-file linear pattern infiltrated around vessels (**e**) and normal ducts (**f**) and infiltrated parallel to the fat border (**g**). A desmoplastic reaction occurred in the centre of the tumour (**h**). The bars are 2 mm (**a**, **c**) and 100 μm (**b**, **d**–**h**)

The protocol for the microscopic maximum tumour size was as follows:

1. After fixation, surgical specimens were cut in parallel into approximately 5-mm-thick slices.
2. The maximum tumour diameter in each cross section was measured.
3. Using a pathological map, the maximum diameter perpendicular to the cross section was measured [16].
4. #2 and #3 were compared, and the largest one was defined as pathological IBC size.

Nuclear pleomorphism, mitotic count, lymphovascular invasion, pectoral muscle invasion and skin invasion were evaluated. ILCs were classified into the following histological subtypes: the classic type, in which more than half of discohesive cells were small and uniform and dispersed individually or arranged in a single-file linear pattern, and others (nonclassic type), including pleomorphic ILC [1, 17]. Immunohistochemistry for oestrogen and progesterone receptors, human epidermal growth factor receptor 2 (HER2) and Ki67 was performed in each laboratory and reevaluated. E-cadherin immunostaining (clone NCH-38, 1:200, Agilent Technologies, Santa Clara, CA, USA) in surgical specimens was performed in all ILCs and IBC-NSTs with a few tubular formations and discohesive cells.

PVI was defined as the infiltration of tumour cells surrounding the vessels distributed in the breast, except for capillaries, which were discontinuous from the main invasion (Supplemental Fig. 1, a). PVI was mostly observed in breast tissue and retromammary fat tissue. PVI also includes infiltration into the collagen fibres surrounding the vessel (**b**). Tumour cells individually infiltrated or formed small clusters (**c**). In the case exhibiting pectoral muscle invasion, PVI was observed beyond the breast (**d**). Tumour cells noncohesively infiltrated surrounding vessels in multiple layers (**e, f**). Tumour cell infiltration was clearly visualized surrounding small vessels and lymph vessels using immunohistochemistry, which was performed using antibodies against cytokeratin (AE1/AE3, F. Hoffmann-La Roche, Ltd., Basel, Switzerland: **g**), CD34 (clone QBEnd/10, Leica Biosystems, Wetzlar, Germany: **h**) and podoplanin (Clone D2-40, 1:4, Nichirei Bioscience Inc., Tokyo, Japan: **i**) with a VENTANA BenchMark ULTRA automated stainer (F. Hoffmann-La Roche, Ltd.). Tumour cells accompanied by lymphovascular invasion or along the long axis of the vessel were also included as PVI, while PVI with coexisting ducts or lobules was excluded. PVI was evaluated using only H&E-stained slides. As intratumoural heterogeneity was observed in the distribution of PVI, the number of PVI was evaluated by the total number of two sections, including the main tumour.

Immunohistochemical staining using an antibody for phospho-myosin light chain 2 (p-MLC2) (1:200; Cell Signalling Technologies, Danvers, MA, USA) was performed manually with BOND Polymer Refine Detection. We evaluated p-MLC2 in 93% (54/58) of ILCs that were suitable for immunostaining for phosphorylation. p-MLC2 was assessed in hotspots located in the invasive front of satellite foci or main tumour in a 100 × field of view and evaluated semiquantitatively using a modified H-score determined by staining intensity and occupancy (%) (H-score = 1 × [% light staining] + 2 × [% moderate staining] + 3 × [% strong staining]) [18]. Staining intensity was graded by comparing endothelial cells and myoepithelial cells with endogenous strong staining. Light staining was defined as faint and heterogeneous cytoplasmic staining. Strong staining showed a similar density of homogeneous cytoplasmic staining to that of endothelial cells. Moderate staining was defined as intermediate cytoplasmic staining between weak and strong staining (Supplemental Fig. 2). The total H-score of the three fields of view was compared.

Axillary treatment

Pathologically, a sentinel lymph node (SLN) with micrometastases (> 0.2 mm and ≤ 2 mm) or macrometastases (> 2 mm) was diagnosed as a positive node [1]. In most clinically node-negative [cN (−)] cases, sentinel node biopsy (SNB) was performed, and axillary lymph node dissection (ALND) was added if macrometastases were detected in the SLN. Notably, two PVI-positive cases and four PVI-negative cases with SLN metastasis, including macrometastases, did not undergo ALND.

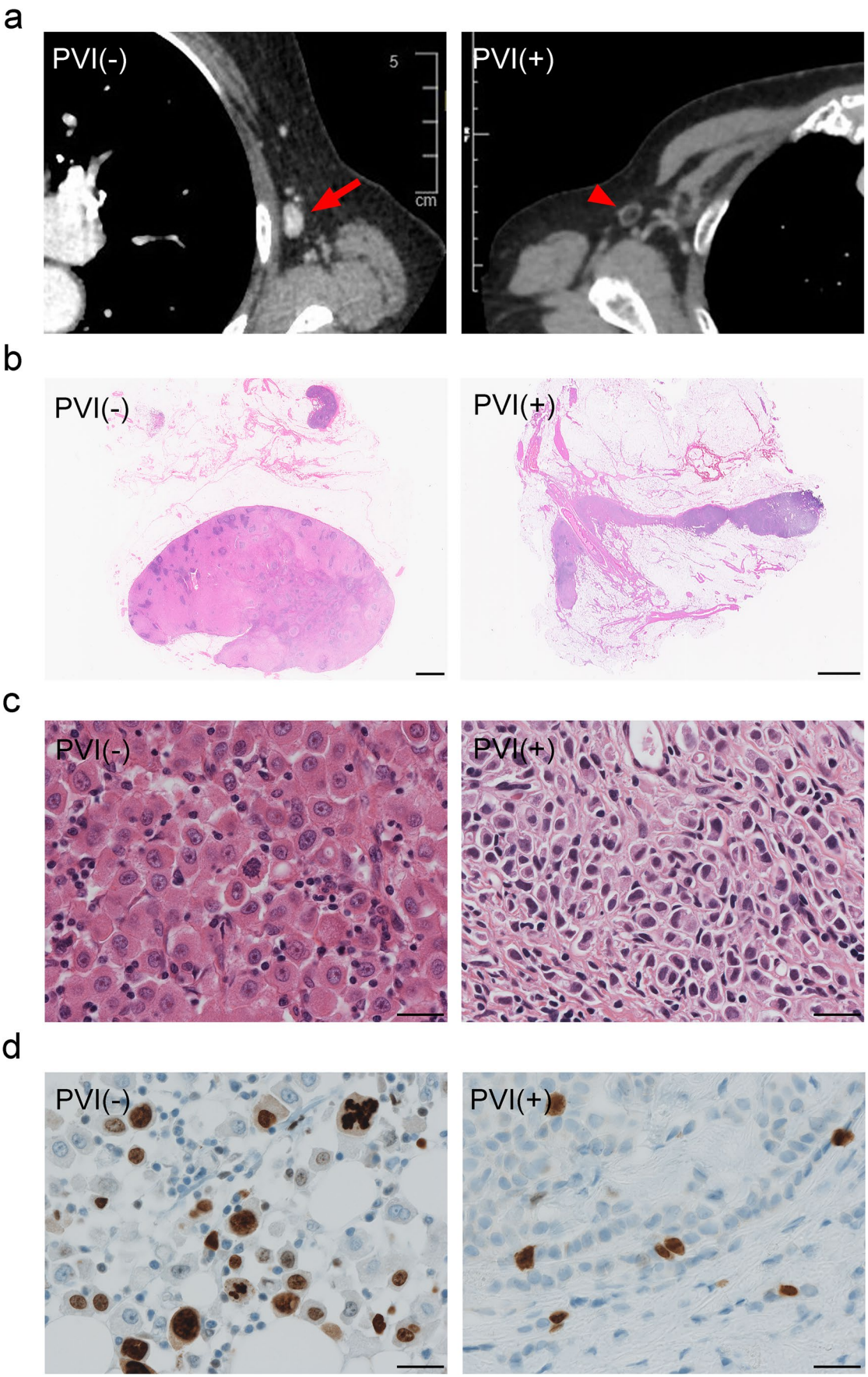
a
PVI(-)
5
cm
PVI(+)
b
PVI(-)
PVI(+)
c
PVI(-)
PVI(+)
d
PVI(-)
PVI(+)

◂**Fig. 2 Morphological differences in metastatic lymph nodes according to PVI.** Representative images of axillary lymph nodes (arrow) lacked intranodal fat density with adenopathy on CT images of PVI-negative cases, while lymph nodes (arrowhead) showed no distinct adenopathy in PVI-positive cases of pN2–pN3 (**a**). Tumour cells expanded in the lymph node showing adenopathy in macroscopic H&E sections of PVI-negative cases, while metastatic lymph nodes showed minimum morphological changes in PVI-positive cases despite pN2–pN3 (**b**). Tumour cells exhibited moderate to marked nuclear pleomorphism and mitosis with eosinophilic abundant cytoplasm diagnosed as pleomorphic type in the lymph node of PVI-negative cases (**c**). In contrast, tumour cells had thin cytoplasm with mild nuclear atypia in the lymph node in PVI-positive cases. The Ki67 index in the tumour cells of the main tumour was significantly higher in PVI-negative cases than in PVI-positive cases when limited to pN2–pN3 (**d**). The bars are 2 mm (**b**) and 25 μm (**c, d**)

Statistical analysis

All statistical analyses were performed using EZR (ver. 1.51, Saitama Medical Center, Jichi Medical University, Saitama, Japan) [19]. Continuous variables were analysed using the Student's *t* test and Mann–Whitney *U* test. Data are expressed as the means with standard deviation (SD) or medians with interquartile range (IQR). Categorical variables were analysed using Fisher's exact test. Any variable with a p value of < 0.05 was considered significant. To match some clinical baseline characteristics of ILCs and IBC-NSTs, the propensity score was estimated by fitting a logistic regression model. One-to-one matching was performed using the nearest neighbour match on the propensity score with calliper width set to 0.20 times the standard deviation of the propensity score.

Results

Clinicopathological characteristics of ILC and IBC-NST (Supplemental Table 1)

A total of 122 cases of IDC and 139 cases of ILC were compared. Age was significantly higher in patients with ILC than in those with IBC-NST ($p < 0.01$). As previously reported, the clinical and pathological tumour size and the frequency of HER2-negative cases were significantly higher in ILCs than in IBC-NSTs ($p < 0.001$). The frequency of PVI was significantly higher in ILCs than in IBC-NSTs (50% vs. 9%; $p < 0.001$). The patients were matched according to the baseline characteristics known to differ between ILCs and IBC-NSTs, such as age, clinical tumour size, clinical node status and oestrogen receptor (ER) and HER2 status [1]. Even in the matched cases, the pathological tumour size of ILCs was larger than that of IBC-NSTs ($p < 0.001$). The frequency of PVI remained higher in ILCs than in IBC-NSTs ($p < 0.001$). The median number of PVIs in two sections was two (range, 1–21) in PVI-positive cases with ILC and one (range, 1–2) in PVI-positive cases with IBC-NSTs.

Clinicopathological characteristics of ILCs with or without PVI (Table 1)

The clinical and pathological tumour sizes were significantly larger in PVI-positive cases than in PVI-negative cases ($p < 0.01$ and $p < 0.001$, respectively). Remarkably, the difference between pathological and clinical tumour size was larger in PVI-positive cases ($p < 0.01$). Pectoral muscle invasion was observed in only three PVI-positive, pathologically node-negative cases despite not being locally advanced cancer with multiple lymph node metastases. There was no difference in age, nuclear pleomorphism, mitotic count, lymphovascular invasion, histological subtype, ER, HER2 status or Ki67 index.

Tumour morphology on imaging (Supplemental Fig. 3)

ILCs are known to show masses as well as non-mass enhancement, such as IBC-NST [20, 21]. In the MR images, PVI-negative cases of ILC typically showed masses with irregular margins (**a**), while PVI-positive cases typically showed non-mass enhancement with segmental distribution (**b**). To clarify the difference in tumour invasion manner according to PVI, the circularity of the tumour was evaluated in the images. In 68 cases evaluated by MRI, the circularity of the tumour in PVI-positive cases was significantly lower than that in PVI-negative cases ($p < 0.01$) (**c**). Similarly, in 79 cases who underwent CT imaging, the circularity was lower in PVI-positive cases ($p < 0.01$) (**d**).

Pathological characteristics of PVI-positive ILCs (Fig. 1)

PVI-negative cases showed tumour growth accompanied by a desmoplastic reaction at the invasive front (**a**). At higher magnification, tumour cells arranged in a single-file linear pattern infiltrated against the surrounding fat accompanied by desmoplastic reactions and disturbance of background architecture (**b**). In contrast, PVI-positive cases showed that small and uniform tumour cells infiltrated into the fibrous connective tissue accompanied by minimum disturbance of background architecture (**c, d**). Tumour cells arranged in a single-file linear pattern infiltrated around vessels (**e**) and normal ducts (**f**) with a few desmoplastic reactions. PVI-positive cases frequently exhibited infiltration surrounding the duct and lobules apart from the main invasion, similar to the so-called concentric (targetoid) pattern [1]. In addition, single-file linear cords of tumour cells were aligned parallel to the fat border (**g**) [22]. Even in PVI-positive cases,

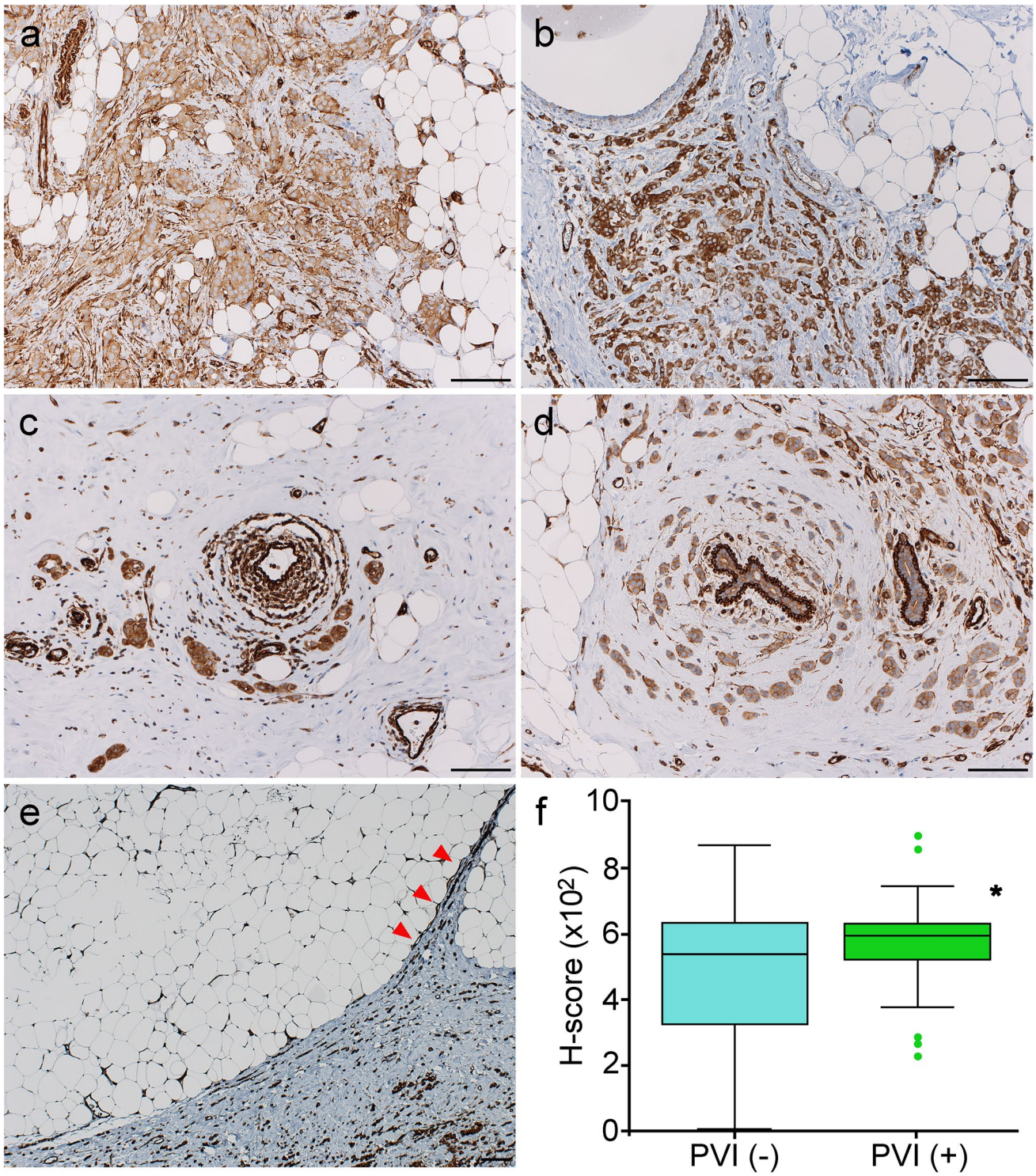

Fig. 3 Myosin II activation of tumour cells with PVI in the invasive front. Tumour cells showed less intense cytoplasmic staining of p-MLC2 than endothelial cells in PVI-negative cases (**a**). Tumour cells showed cytoplasmic staining of p-MLC2 as strong as that of endothelial cells in PVI-positive cases (b). Tumour cells surrounding the vessel (**c**) and the duct (**d**) showed similar intensity of staining to that of endothelial cells and myoepithelial cells in PVI-positive cases. Parallel infiltration of p-MLC2-positive tumour cells along the fat border is shown (**e**). Notably, tumour cells infiltrated along the small vessels without destruction of the preexisting structure (arrowheads) in the upper right. PVI-positive cases showed a higher total H-score of p-MLC2 staining than PVI-negative cases (**f**) (Student's *t* test, $^{*}p < 0.05$). The bar is 100 μm

desmoplastic reactions were often observed in the centre of the tumour (**f**).

Discrepancy between the clinical and pathological lymph node status in PVI-positive cases (Fig. 2)

There was no difference in clinical and pathological node status between patients with and without PVI (Table 1). However, when limited to cN(−) ILCs, the frequency of pN2-pN3 (4 or more positive nodes) cases was significantly higher in PVI-positive cases than in PVI-negative cases (15.2% vs. 0%; $p < 0.01$) (Table 2). Furthermore, when limited to cN(−) but pN(+) cases, the frequency of pN2–pN3 was higher in PVI-positive cases than in PVI-negative cases (45.5% vs. 0%; $p < 0.05$).

These results indicated that the axillary lymph nodes might be diagnosed as cN(−) in image analysis due to trivial morphological changes in pN2–pN3 cases with PVI. Indeed, for the clinical node size, the short-axis diameter or cortical thickness was significantly smaller in PVI-positive cases than in PVI-negative cases in pN2–pN3 cases ($p < 0.05$) (**a,b**, Supplemental Table 2). Conversely, there was no difference in the pathologically maximum metastatic size. Regarding histological subtype, the classic type of ILCs was predominant in pN2–pN3 cases with PVI compared with pN2–pN3 cases without PVI ($p < 0.01$). On the other hand, pleomorphic ILCs with apocrine features were frequently observed in pN2–pN3 cases without PVI ($p < 0.05$) (**c**, Supplemental Table 2). pN2–pN3 cases with PVI showed a significantly lower Ki-67 index than the matched cases without PVI ($p < 0.01$) (**d**, Supplemental Table 2).

Phospho-MLC2 expression in ILCs at the invasive front (Fig. 3)

To compare the differences in migration mode with or without PVI, we evaluated p-MLC2, which is one of the indicators of myosin II activation. Myosin II activity reflects the contraction of actomyosin, which is the main mechanism eliciting ameboid migration. Tumour cells exhibited mild to moderate cytoplasmic staining in the invasive front of the PVI-negative cases (**a**). In contrast, tumour cells in the invasive front showed intense cytoplasmic staining similar to that of endothelial cells in the PVI-positive cases (**b**). Tumour cells surrounding the vessel (**c**) and the duct (**d**), particularly discohesive cells, also showed strong staining similar to endothelial cells or myoepithelial cells. Tumour cells individually infiltrating along the fat border and capillaries showed a strong positive reaction for p-MLC2 (**e**). The total H-score from p-MLC2 staining was significantly higher in the invasive front in PVI-positive cases than in PVI-negative cases ($p < 0.05$) (**f**).

Discussion

In this study, PVI was identified as a more common finding in ILCs than in IBC-NSTs. PVI in ILCs was associated with extensive tumour infiltration, which was related to subclinical lymph node metastasis without adenopathy. Myosin II activity was higher in the tumour margins of ILCs with PVI, suggesting that PVI may be caused by ameboid migration. These results supported our hypothesis that PVI was associated with the unique tumour behaviour of ILCs.

PVI was defined as the infiltration of tumour cells surrounding the vessel apart from the main tumour in this study. Infiltration surrounding ducts and lobules and parallel infiltration to the fat border were also frequently observed in PVI-positive cases. As represented by these infiltrations, the tumour cells in PVI-positive cases penetrated surrounding tissues, which was rarely accompanied by desmoplastic reaction and disturbance of background collagen structure. Recent 2D/3D approaches strongly suggest that tumour invasion is guided and supported by preexisting anatomic structures, including vessels and collagen fibre bundles [6]. The tumour cells in PVI-positive cases might use these gaps in the preexisting fibre bundles with individual cell or single-file linear patterns. Furthermore, the tumour cells showed dominant ameboid migration in the invasive front, where cytoplasm could be squeezed between tissue gaps without proteolysis. In PVI-positive cases, these mechanisms would enable tumour cells to infiltrate the stroma without disturbing the background collagen structure.

In several types of tumours known to have PVI, including ILCs, the Rho-Rock pathway is activated [10, 23, 24]. Rock can phosphorylate MLC2 directly and indirectly. Consequently, high myosin II activation promotes a high level of actomyosin contraction, which is the key to ameboid migration. In particular, Georgouli et al. reported that the invasive fronts of melanoma were enriched in myosin II-activated rounded-ameboid cancer cells, which secrete cytokines and autoactivate Rock-myosin II [25]. In this study, myosin II activation was significantly higher in the invasive front in PVI-positive cases. High myosin II activation was also observed in infiltration surrounding ducts and parallel infiltration to the fat border, which were distinctive findings of ILCs with PVI. These findings may suggest that ILCs assume modes of infiltration, i.e. ameboid and mesenchymal migration, differently in the microenvironment or with genetic changes.

Recent randomized clinical trials reported that SLN-positive, clinically node-negative patients did not have an inferior prognosis even if ALND was omitted [26–28]. However, some studies have reported that SLN-positive ILCs had a greater number of pathologically positive nodes than IBC-NSTs [29–31]. In this study, there was no difference in

pathological node metastasis and lymphovascular invasion between all ILCs with or without PVI. However, when limited to cN(–) cases, there were significantly more pN2–pN3 cases amongst the PVI-positive cases. One of the reasons is that the metastatic lymph nodes did not clinically show adenopathy. Although the mechanism of minimum lymphadenopathy is still unknown, the low Ki67 proliferation index of the main tumour and reduced stromal reaction in the invasive front may be associated with metastasis without adenopathy. Therefore, omitting ALND for SLN-positive cases with PVI in ILC may lead to inadequate adjuvant therapy due to uncertain staging and worse prognosis.

In PVI-positive cases, the pathological tumour size was significantly larger than the clinical tumour size. The tumour cells in PVI-positive cases extensively infiltrated the surrounding ducts and lobules and aligned in parallel to the fat border individually and in a single-file linear pattern without disturbance of the background collagen structure. Because such a mode of infiltration elicits fewer deviations from the normal structures on imaging [32], this may make it more difficult to evaluate precise tumour extension. These characteristics of infiltration with PVI also reflected the tumour morphology of the images. The lower circularity in PVI-positive cases was assumed to be not only due to PVI-related irregularity but also due to the segmental distributions related to infiltration around ducts and parallel infiltration to the fat border, even though there was little intraductal spread. On the other hand, the higher circularity in PVI-negative cases was assumed to be solitary masses, even with irregular and spiculated margins.

This study had limitations. First, because of the multi-institutional retrospective nature of the study, preoperative imaging with or without MRI was not unified. Therefore, the circularity was verified not only by MRI but also by CT images. Second, most of the specimens for p-MLC2 immunostaining were partially dissected and fixed for the evaluation of HER2 staining, so they could not be unified to be representative true invasive fronts. Third, not all ILCs in stages I–III were included because cases with neoadjuvant therapy were excluded from this study. Particularly, PVI-negative cases with clinically many lymphadenopathies may have been treated with neoadjuvant chemotherapy, which may have resulted in fewer pN2–pN3 cases.

In conclusion, our study revealed that PVI is a distinct pathological finding identified in ILCs that can be evaluated by imaging. Myosin II activity was higher in the tumour margins of ILCs with PVI, suggesting that PVI may be caused by ameboid migration. PVI could be a predictor for clinically node-negative pN2–pN3 cases using clinical tumour size and circularity, which may help surgeons decide whether ALND should be performed for staging in ILC. In the future, determination of the specific cutoff values for the circularity and clinical tumour size for diagnosis of ILCs using clinical images and evaluation of the relationship between PVI and prognosis for understanding ILC-specific behaviour can be useful.

Supplementary Information The online version contains supplementary material available at https://doi.org/10.1007/s00428-022-03391-8.

Acknowledgements Technical assistance from Ms. Saori Ogasawara, Saeko Osanai, Misato Sakamoto and Hiroko Mori of the Department Pathology and Molecular Medicine of Hirosaki University Graduate of Medicine is highly appreciated.

Author contribution **Conceptualization**: AI, HM, KH; **methodology**: AI, HM, KK, YT; **formal analysis and investigation**: AI, HM, KK, YT, XP, TS; **visualization**: AI, KK, TS; **writing—original draft preparation**: AI; **writing—review and editing**: HM, KH; **supervision**: HM, KH.

Data availability The datasets generated during and/or analysed during the current study are available from the corresponding author on reasonable request.

Declarations

Ethics approval and consent to participate This article does not contain any studies with human participants or animals performed by any of the authors. For this type of study, formal consent was not needed.

Conflict of interest The authors declare no competing interests.

References

1. WHO Classification of Tumours Editorial Board (2019) Breast tumours. WHO clasification of tumours series, 5th ed. vol.2. International Agenc for Reseaarch on Cancer, Lyon, pp 114–118
2. Ciriello G, Gatza ML, Beck AH, Wilkerson MD, Rhie SK, Pastore A et al (2015) Comprehensive molecular portraits of invasive lobular breast cancer. Cell 163:506–519
3. Johnson K, Sarma D, Hwang ES (2015) Lobular breast cancer series: imaging. Breast Cancer Res 17:94. https://doi.org/10.1016/j.cell.2015.09.033
4. Hoda SA, Brogi E, Koerner FC, Rosen PP (2014) Rosen's breast pathology, 4th edition. Wolters Kluwer, Alphen Aan Den Rijn, pp 855–892
5. Morrow E, Lannigan A, Doughty J, Litherland J, Mansell J, Stallard S et al (2018) Population-based study of the sensitivity of axillary ultrasound imaging in the preoperative staging of node-positive invasive lobular carcinoma of the breast. Br J Surg 105:987–95. https://doi.org/10.1002/bjs.10791
6. Friedl P, Alexander S (2011) Cancer invasion and the microenvironment: plasticity and reciprocity. Cell 147:992–1009. https://doi.org/10.1016/j.cell.2011.11.016
7. Pandya P, Orgaz JL, Sanz-Moreno V (2017) Modes of invasion during tumour dissemination. Mol Oncol 11:5–27. https://doi.org/10.1002/1878-0261.12019

8. Foschini MP, Righi A, Cucchi MC, Ragazzini T, Merelli S, Santeramo B et al (2006) The impact of large sections and 3D technique on the study of lobular in situ and invasive carcinoma of the breast. Virchows Arch 448:256–61. https://doi.org/10.1007/s00428-005-0116-y
9. Baker GJ, Yadav VN, Motsch S, Koschmann C, Calinescu AA, Mineharu Y et al (2014) Mechanisms of glioma formation: iterative perivascular glioma growth and invasion leads to tumor progression, VEGF-independent vascularization, and resistance to antiangiogenic therapy. Neoplasia 16:543–61. https://doi.org/10.1016/j.neo.2014.06.003
10. Hirata E, Yukinaga H, Kamioka Y, Arakawa Y, Miyamoto S, Okada T et al (2012) In vivo fluorescence resonance energy transfer imaging reveals differential activation of Rho-family GTPases in glioblastoma cell invasion. J Cell Sci 125:858–68. https://doi.org/10.1242/jcs.089995
11. Lugassy C, Zadran S, Bentolila LA, Wadehra M, Prakash R, Carmichael ST et al (2014) Angiotropism, pericytic mimicry and extravascular migratory metastasis in melanoma: an alternative to intravascular cancer dissemination. Cancer Microenviron 7:139–52. https://doi.org/10.1007/s12307-014-0156-4
12. Lugassy C, Kleinman HK, Vermeulen PB, Barnhill RL (2020) Angiotropism, pericytic mimicry and extravascular migratory metastasis: an embryogenesis-derived program of tumor spread. Angiogenesis 23:27–41. https://doi.org/10.1007/s10456-019-09695-9
13. Shien T, Akashi-Tanaka S, Yoshida M, Hojo T, Iwamoto E, Miyakawa K et al (2008) Evaluation of axillary status in patients with breast cancer using thin-section CT. Int J Clin Oncol 13:314–9. https://doi.org/10.1007/s10147-007-0753-z
14. Takashimizu Y, Iiyoshi M (2016) New parameter of roundness R: circularity corrected by aspect ratio. Prog in Earth and Planet Sci. 3
15. Fitzgibbons PL, Connolly JL, With guidance from the CAP Cancer and CAP Pathology Electronic Reporting Committees. (2022) Protocol for the examination of resection specimens from patients with invasive carcinoma of the breast, College of American Pathologists (CAP), Version: Breast Invasive Resection 4.6.0.0, pp 23–25
16. Inoue T, Tamaki Y, Hamada S, Yamamoto S, Sato Y, Tamura S et al (2005) Usefulness of three-dimensional multidetector-row CT images for preoperative evaluation of tumor extension in primary breast cancer patients. Breast Cancer Res Treat 89:119–125. https://doi.org/10.1007/s10549-004-1477-7
17. Iorfida M, Maiorano E, Orvieto E, Maisonneuve P, Bottiglieri L, Rotmensz N et al (2012) Invasive lobular breast cancer: subtypes and outcome. Breast Cancer Res Treat 133:713–23. https://doi.org/10.1007/s10549-012-2002-z
18. Rodriguez-Hernandez I, Maiques O, Kohlhammer L, Cantelli G, Perdrix-Rosell A, Monger J et al (2020) WNT11-FZD7-DAAM1 signalling supports tumour initiating abilities and melanoma amoeboid invasion. Nat Commun 11:5315. https://doi.org/10.1038/s41467-020-18951-2
19. Kanda Y (2013) Investigation of the freely available easy-to-use software 'EZR' for medical statistics. Bone Marrow Transplant 48:452–8. https://doi.org/10.1038/bmt.2012.244
20. Mann RM, Hoogeveen YL, Blickman JG, Boetes C (2008) MRI compared to conventional diagnostic work-up in the detection and evaluation of invasive lobular carcinoma of the breast: a review of existing literature. Breast Cancer Res Treat 107:1–14. https://doi.org/10.1007/s10549-007-9528-5
21. Morris EA, Comstock CE, Lee CH (2013) ACR BI-RADS® magnetic resonance imaging. In: ACR BI-RADS® Atlas, Breast imaging reporting and data system. American College of Radiology, Virginia, pp 15–37
22. Christgen M, Steinemann D, Kuhnle E, Langer F, Gluz O, Harbeck N et al (2016) Lobular breast cancer: clinical, molecular and morphological characteristics. Pathol Res Pract 212:583–97. https://doi.org/10.1016/j.prp.2016.05.002
23. Schackmann RC, van Amersfoort M, Haarhuis JH, Vlug EJ, Halim VA, Roodhart JM et al (2011) Cytosolic p120-catenin regulates growth of metastatic lobular carcinoma through Rock1-mediated anoikis resistance. J Clin Invest. 121:3176–88. https://doi.org/10.1172/JCI41695
24. Pramod N, Nigam A, Basree M, Mawalkar R, Mehra S, Shinde N, et al. (2021) Comprehensive review of molecular mechanisms and clinical features of invasive lobular cancer. Oncologist 26:e943–e953. https://doi.org/10.1002/onco.13734
25. Georgouli M, Herraiz C, Crosas-Molist E, Fanshawe B, Maiques O, Perdrix A et al (2019) Regional activation of myosin II in cancer cells drives tumor progression via a secretory cross-talk with the immune microenvironment. Cell 176(757–74):e23. https://doi.org/10.1016/j.cell.2018.12.038
26. Giuliano AE, Hunt KK, Ballman KV, Beitsch PD, Whitworth PW, Blumencranz PW et al (2011) Axillary dissection vs no axillary dissection in women with invasive breast cancer and sentinel node metastasis: a randomized clinical trial. JAMA 305:569–75. https://doi.org/10.1001/jama.2011.90
27. Giuliano AE, Ballman KV, McCall L, Beitsch PD, Brennan MB, Kelemen PR et al (2017) Effect of axillary dissection vs no axillary dissection on 10-year overall survival among women with invasive breast cancer and sentinel node metastasis: the ACOSOG Z0011 (Alliance) randomized clinical trial. JAMA 318:918–26. https://doi.org/10.1001/jama.2017.11470
28. Donker M, van Tienhoven G, Straver ME, Meijnen P, van de Velde CJH, Mansel RE et al (2014) Radiotherapy or surgery of the axilla after a positive sentinel node in breast cancer (EORTC 10981–22023 AMAROS): a randomised, multicentre, open-label, phase 3 non-inferiority trial. Lancet Oncol 15:1303–10. https://doi.org/10.1016/S1470-2045(14)70460-7
29. Roberts A, Nofech-Mozes S, Youngson B, McCready DR, Al-Assi M, Ramkumar S et al (2015) The importance of applying ACOSOG Z0011 criteria in the axillary management of invasive lobular carcinoma: a multi-institutional cohort study. Ann Surg Oncol 22:3397–401. https://doi.org/10.1245/s10434-015-4756-0
30. Adachi Y, Sawaki M, Hattori M, Yoshimura A, Gondo N, Kotani H et al (2018) Comparison of sentinel lymph node biopsy between invasive lobular carcinoma and invasive ductal carcinoma. Breast Cancer 25:560–5. https://doi.org/10.1007/s12282-018-0852-x
31. Van Wyhe RD, Caudle AS, Shaitelman SF, Perkins GH, Buchholz TA, Hoffman KE et al (2018) A component of lobular carcinoma in clinically lymph node-negative patients predicts for an increased likelihood of upstaging to pathologic stage III breast cancer. Adv Radiat Oncol 3:252–7. https://doi.org/10.1016/j.adro.2018.02.007
32. Izumori A, Horii R, Akiyama F, Iwase T (2013) Proposal of a novel method for observing the breast by high-resolution ultrasound imaging: understanding the normal breast structure and its application in an observational method for detecting deviations. Breast Cancer 20:83–91. https://doi.org/10.1007/s12282-011-0313-2

Supplemental Table 1. Clinicopathological characteristics of ILC and IDC.

Characteristics	ILC (n=139)	IBC-NST (n=122)	*p* value	Matched ILC (n=70)	Matched IBC-NST (n=70)	*p* value
Age(years)	60.2±12.0	56.1±11.7	<0.01	58.6±10.8	59.8±11.2	0.51
Clinical tumor size (mm)	29.5 ± 16.5	18.1 ± 11.6	<0.001	23.3±12.5	21.3±12.3	0.35
Clinical node status			0.66			0.53
Negative	92.1%(128/139)	90.2%(110/122)		90.0%(63/70)	94.3%(66/70)	
Positive	7.9%(11/139)	9.8%(12/122)		10.0%(7/70)	5.7%(4/70)	
Estrogen receptor			0.06			0.53
Negative	6.5%(9/139)	13.9%(17/122)		10.0%(7/70)	5.7%(4/70)	
Positive	93.5%(130/139)	86.1%(105/122)		90.0%(63/70)	94.3%(66/70)	
HER2 status			<0.001			1.00
Negative	97.1%(135/139)	81.1%(99/139)		95.7%(67/70)	97.1%(68/70)	
Positive	2.9%(4/139)	18.9%(23/139)		4.3%(3/70)	2.9%(2/70)	
Pathological tumor size (mm)	33.4 ± 22.5	15.1 ± 9.6	<0.001	30.8 ± 17.8	17.0± 10.6	<0.001
Pathological node status			0.90			1.00
Negative	68.3%(95/139)	67.2%(82/122)		65.7%(46/70)	65.7%(46/70)	
Positive	31.7%(44/139)	32.8%(40/122)		34.3%(24/70)	34.3%(24/70)	
Lymphovascular invasion			0.21			0.82
Negative	84.2%(117/139)	77.9%(95/122)		84.3%(59/70)	81.4%(57/70)	
Positive	15.8%(22/139)	22.1%(27/122)		15.7%(11/70)	18.6%(13/70)	
PVI			<0.001			<0.001
Negative	49.6%(69/139)	91.0%(111/122)		55.7%(39/70)	87.1%(61/70)	
Positive	50.4%(70/139)	9%(11/122)		44.3%(31/70)	12.9%(9/70)	

ILC: invasive lobular carcinoma, IBC-NST: invasive breast carcinoma of no special type, HER2: human epidermal growth factor receptor 2: PVI: perivascular infiltration. Values were presented as mean ± SD.

Supplemental Table 2. Clinicopathological characteristics of pN2-pN3 ILC with PVI.

	pN2+pN3 ILC (n=19)		*p* value
	PVI(-) (n=6)	PVI(+) (n=13)	
Clinical size of LN (mm)	8.6 (7.1-10.8)	6.0 (4.0-6.9)	0.017
Pathological metastatic size of LN (mm)	11.5 (7.3-18.3)	11.0 (6.0-15.0)	0.57
Histological subtype			
Classic	16.7%(1/6)	84.6%(11/13)	0.009
Pleomorphic	50.0%(3/6)	0%(0/13)	0.021
ER-positive and HER2-negative	50.0%(3/6)	92.3% (12/13)	0.071
Ki67 index (%)	31(22-38)	11 (6-19)	0.003

LN, lymph node: ER, estrogen receptor: HER2, human epidermal growth factor receptor 2. Values are expressed as median (Inter-Quartile Range).

Supplemental Figure 1

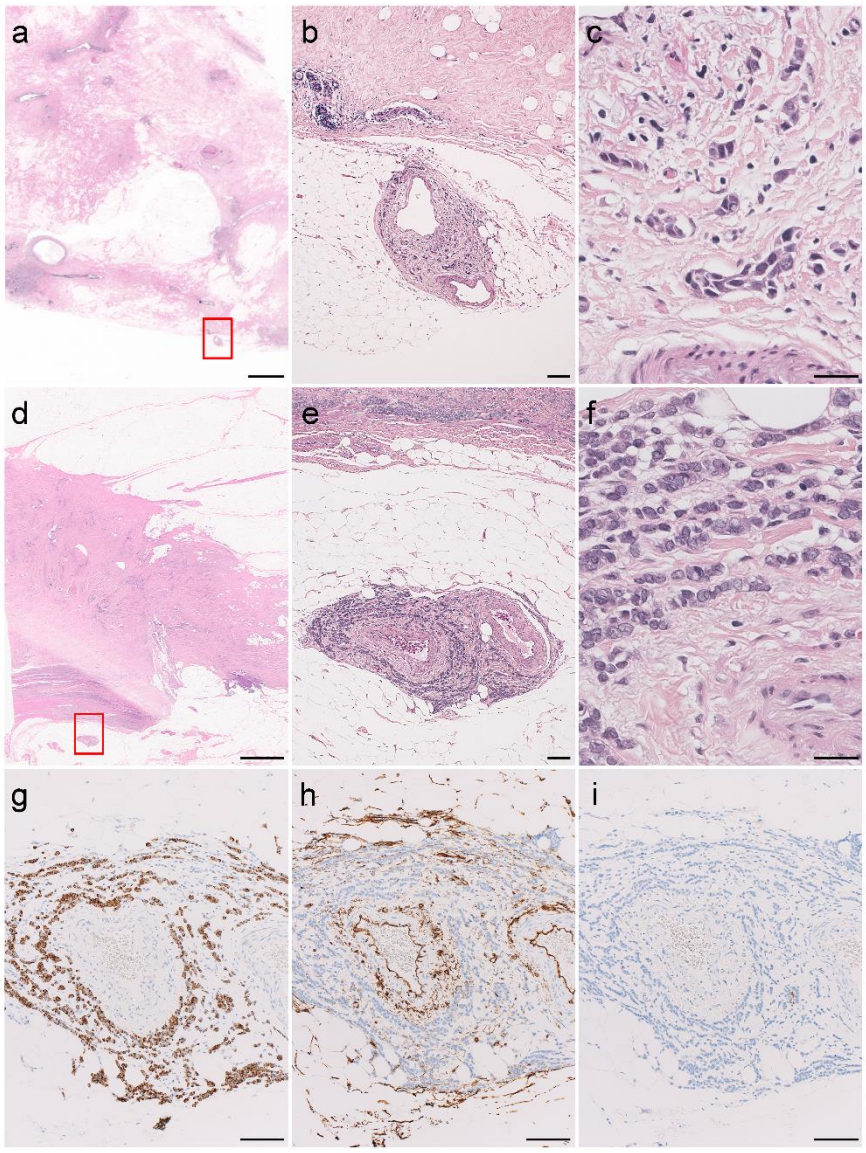

Supplemental Figure 1. Pathological definition of perivascular infiltration (PVI) in ILC.
At low magnification, discontinuous lesions apart from the main tumor were detected in the retromammary fat tissue (red rectangles) (**a**). In the red rectangular area, tumor cells infiltrated surrounding vessels (**b**). Tumor cells exhibited a thin rim of cytoplasm, which is a typical pathological characteristic of classic ILCs (**c**). In the case exhibiting pectoral muscle invasion, PVI was observed beyond the breast (red rectangle) (**d**). Similar to B, tumor cells also infiltrated into the perivascular space with poor stromal reaction in the red rectangle (**e**). At higher magnification, tumor cells showing thin cytoplasm infiltrated discohesively (**f**). Infiltration of tumor cells surrounding vessels and lymph vessels was confirmed by immunohistochemistry for AE1/AE3 (**g**), CD34 (**h**) and D2-40 (**i**). The bar is 2 mm (**a, d**) and 100 μm (**b,e,g-i**), 25 μm (**c,f**).

Supplemental Figure 2.

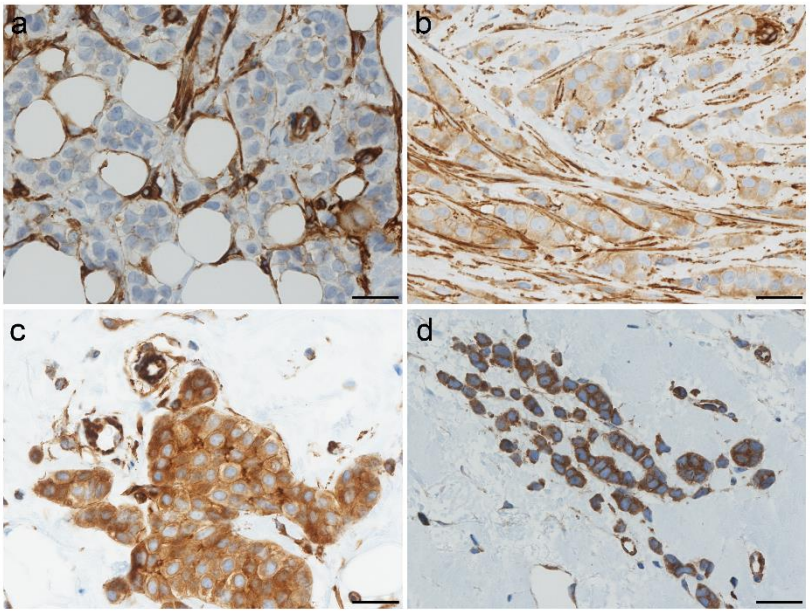

Supplemental Figure 2. Intensity score of phopho-MLC2.

(**a**) score 0 (no staining), (**b**) score 1 (light staining), (**c**) score 2 (moderate staining), and (**d**) score 3 (strong staining). The bar is 25 mm.

Supplemental Figure 3.

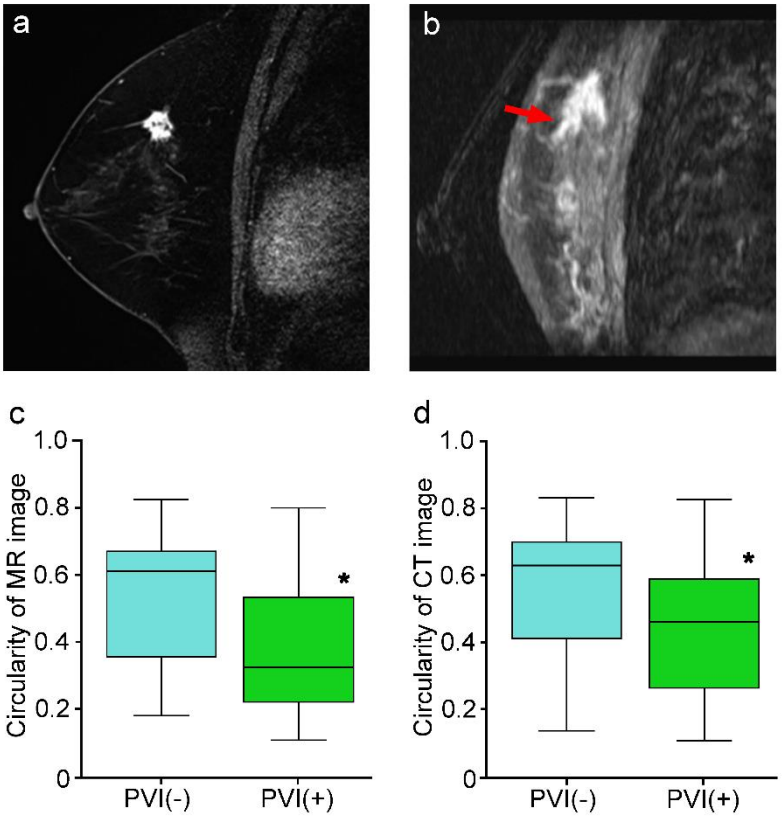

Supplemental Figure 3. Difference in tumor morphology in the images.

The PVI-negative case showed a lobulated mass with irregular and spiculated margins in MR imaging (circularity = 0.58) (**a**). The PVI-positive case showed non-mass enhancement with segmental distribution and conspicuously irregular borders in the MR image (circularity=0.32) (**b**). The circularity for the tumors in PVI-positive cases was significantly lower than that in PVI-negative cases in both MRI (**c**) and CT (**d**) images (Mann–Whitney U test, *p < 0.01).